Eur Biophys J (2003) 32: 635–643
DOI 10.1007/s00249-003-0326-7

ARTICLE

Florian Schapper · José Tiago Gonçalves · Martin Oheim

Fluorescence imaging with two-photon evanescent wave excitation

Received: 20 December 2002 / Accepted: 2 May 2003 / Published online: 3 September 2003

Abstract We demonstrate broad-field, non-scanning, two-photon excitation fluorescence (2PEF) close to a glass/cell interface by total internal reflection of a femtosecond-pulsed infrared laser beam. We exploit the quadratic intensity dependence of 2PEF to provide non-linear evanescent wave (EW) excitation in a well-defined sample volume and to eliminate scattered background excitation. A simple model is shown to describe the resulting 2PEF intensity and to predict the effective excitation volume in terms of easily measurable beam, objective and interface properties. We demonstrate non-linear evanescent wave excitation at 860 nm of acridine orange-labelled secretory granules in live chromaffin cells, and excitation at 900 nm of TRITC-phalloidinactin/GPI-GFP double-labelled fibroblasts. The confined excitation volume and the possibility of simultaneous multi-colour excitation of several fluorophores make EW 2PEF particularly advantageous for quantitative microscopy, imaging biochemistry inside live cells, or biosensing and screening applications in miniature high-density multi-well plates.

Keywords Evanescent wave excitation · Microscopy · Non-linear excitation · Total internal reflection fluorescence microscopy · Two-photon excitation fluorescence

This paper is dedicated to the memory of Prof. Horst Harreis (1940–2002)

F. Schapper · J. T. Gonçalves · M. Oheim (✉)
Neurophysiology and New Microscopies,
Ecole Supérieure de Physique et Chimie Industrielles (ESPCI),
10 rue Vauquelin, 75005 Paris, France
E-mail: martin.oheim@espci.fr
Tel.: +33-1-40794665
Fax: +33-1-40794760

J. T. Gonçalves
Molecular Biology of Neuronal Signals,
Max-Planck-Institute for Experimental Medicine,
Hermann-Rein Strasse 3, 37075 Göttingen, Germany

Abbreviations 1PEF: one-photon excited fluorescence · 2PEF: two-photon excited fluorescence · APD: avalanche photo diode · CHO: Chinese hamster ovary · DMEM: Dulbecco's modified Eagle's medium · EGFP: enhanced green fluorescent protein · EW: evanescent wave · FCS: fetal calf serum · GPI: glycosylphosphatidylinositol · TIR: total internal reflection

Introduction

Total internal reflection (TIR) spectroscopy (Harrick 1967) and microscopy (Axelrod 1989) take advantage of the spatial confinement of the evanescent wave to study concentration profiles of fluorophores (Thompson et al. 1993) or scatterers (Chew et al. 1979) close to a dielectric interface. The limited probe distance of the evanescent wave (EW) provides the basis for low-background measurements without interference from deeper sample regions and permits the observation of individual fluorophore dynamics (Funatsu et al. 1997; Seitz et al. 2002), even in living cells (Sonnleitner et al. 2002). Improved labelling with genetically targeted fluorophores and technical advances (Axelrod 2001a; Kawano et al. 2001) have recently renewed interest in EW imaging in biophysics (Thompson and Lagerholm 1997), cell biology (Axelrod 2001b; Steyer and Almers 2001; Toomre and Manstein 2001) and biosensing applications (Epstein et al. 2002).

EW imaging of biological samples poses some unique experimental problems associated with the presence of scattered photons. Scattering creates non-vanishing real components of the wave vector in the direction of the surface normal, causing excitation photons to "leak" into deeper sample regions and the fluorescence signal to contain both near- and far-field components (Oheim and Stühmer 2000; Loerke et al. 2002; Rohrbach 2000).

In this paper, we exploit the quadratic intensity dependence of two-photon excitation of fluorescence (2PEF; Denk et al. 1990) to confine fluorescence excitation to a planar near-interface region where the photon

density is high. A simple model predicts the 2PEF excitation volume from measurable set-up parameters. This volume is fairly insensitive to sample turbidity. Finally, we demonstrate that this new imaging technique produces images in live cells and permits simultaneous excitation of several fluorophores for multi-parameter imaging.

Materials and methods

Cell culture and labelling

Bovine chromaffin cells were prepared as described (Darchen et al. 1990) and maintained for 2–3 days in DMEM, 10% FCS, 10 μM fluorodeoxyuridine, 10 μM cytosine/arabinosine and 0.1% streptomycin/penicillin (all from Gibco, Invitrogen, Paisley, Scotland, UK) after plating. We labelled secretory granules with acridine orange (3 min, 5 μM), a weak base that stains acidic intracellular compartments (Sigma, St. Louis, Mo., USA).

Swiss 3T3 fibroblasts were cultured in DMEM, supplemented with 10% FCS and 0.1% streptomycin/penicillin (Gibco). For cytoskeleton-membrane double staining, cells were transfected 24 h after plating with the lipid-raft protein marker GPI-eGFP cDNA (a gift from Dr. P. Verkade, Max-Planck Institute for Cell Biology and Genetics, Dresden, Germany) using the FuGENE 6 transfection reagent (Roche, Mannheim, Germany). 20–22 h later, cells were fixed for 30 min with 4% paraformaldehyde in PBS, permeabilized with 0.1% Triton-X100 for 5 min, and subsequently blocked with 0.2% gelatin in PBS (PBSG) for 10 min. Finally, cells were labelled with 2.5 ng/mL phalloidin-TRITC (Sigma) in PBSG for 45 min and observed after washing.

For imaging, coverslips were rinsed with the standard recording solution, containing (in mM): 145 NaCl, 10 HEPES (pH 7.2), 2.8 $MgCl_2$, 2 $CaCl_2$. Cells were viewed on a custom microscope with bright-field illumination and epifluorescence excitation (TILL, Gräfelfing, Germany) prior to EW imaging to confirm cell adhesion and fluorescent labeling, respectively. Experiments were performed at room temperature (22–23 °C).

Linear and non-linear EW fluorescence excitation

The beams of a 5-W solid-state pumped femtosecond-pulsed Ti:sapphire laser (Spectra-Physics, Mountain View, Calif., USA; ~100 fs pulses at 81 MHz, see figures for excitation wavelengths) and an Ar^+-ion laser (488 nm, Reliant 150, LaserPhysics, West Jordan, Utah, USA) were attenuated to <5 mW and <1 mW average power, respectively, spatially filtered and expanded to have a half width w_0. Both beams were combined and focused by a $f_{FL}=$ 300 mm achromatic doublet (L1 in Fig. 1A; Linos Photonics, Göttingen, Germany) to arrive parfocally and coaxially in the lower objective's back focal plane (BFP; Olympus 60× NA 1.45 PlanApochromat, Hamburg, Germany). A beam focused to the back focal plane of the lower objective (Fig. 1B) results in a parallel beam with half-width $w_r = \emptyset_{pupil} w_o/(2f_{FL})$ (see Appendix). The radial position of a light ray in the objective's BFP determines the angle $\vartheta = \arcsin\left(M\rho/(n_{2,m\omega} f_{TL})\right)$ at which the beam emerges from the objective and onto the interface, as well as its cross-sectional area $\pi w_r^2/(\cos\vartheta)$ in the specimen plane (Fig. 1C; see Appendix for details).

We regulated the micrometer screw that displaced mirror M1 by a two-point calibration. We centred at normal beam incidence ($\vartheta = 0°$, epifluorescence excitation) a second NA-1.45 objective, mounted on an x,y translation stage, with respect to the lower objective (see Fig. 1A). We next defined $\rho_{c,m\omega}$ by increasing ϑ until we observed total internal reflection at the critical angle, $\vartheta_{c,m\omega}$, as a drop in transmitted light intensity.

To measure EW penetration into the sample, we exploited the proportionality of the total amount of fluorescence generated to the penetration depth $w_{z,m\omega}(\vartheta)$:

$$F(\vartheta) \propto \int_0^\infty I^m(z;\vartheta)\,\mathrm{d}z = m^{-1} I^m(0;\vartheta) w_{z,m\omega}(\vartheta) \quad (1)$$

Here, we assume $I^m(z) = I^m(0)\exp\left(-mz/w_{z,m\omega}\right)$, a homogeneous thick $\left(d \gg w_{z,m\omega}(\vartheta)\right)$ sample, and neglected the interaction of the molecular dipoles with the dielectric interface (Mertz 2000). Experimentally, we measured the generated fluorescence in a "thick" ($d \gg w_z$) homogeneous sample, consisting of a 100-μM fluorescein layer, sandwiched between two coverglasses separated by a thin Teflon spacer (Fig. 1). On a plot of measured fluorescence $F(\vartheta)$ vs. $I^m(0;\vartheta)$ the slope is, up to a constant incorporating m, as well as instrument and fluorophore parameters, equal to $w_{z,m\omega}(\vartheta)$. We calculated $I^m(0;\vartheta)$ from the measured value of $I^m\left(0;\vartheta_c^-\right)$, where ϑ_c^- is an angle just below the critical angle (Axelrod et al. 1984).

Fluorescence collection

Fluorescence was collected through the lower objective, extracted with a custom polychroic mirror (AHF, Tübingen, Germany) and was, after appropriate filtering (Chroma, Brattleboro, Vt., USA), imaged on a back-illuminated frame-transfer camera (Photometrics Quantix EEV57-FT, Roper Scientific, Tucson, Ariz., USA). A 488-nm rugate notch filter (1PEF, Barr, Westford, Mass., USA) and a BG-22 absorption filter (2PEF, Chroma) attenuated the reflected laser light. Image acquisition was 50 ms unless otherwise stated. We used Metamorph (Universal Imaging, Downington, Pa., USA) and IGOR (Wavemetrics, Lake Oswego, Ore., USA) software. Fluorescence intensities were expressed as counts per second (cps), one count representing one A/D unit.

Results

Evanescent wave 2PEF does not require beam scanning

We begin by defining the parameters that characterize the excitation volume as well as the resultant fluorescence intensity. 2PEF requires high instantaneous intensities, typically $\sim 10^{20}$ photons/(cm^2 s). These high photon densities are usually achieved in the tight focus of a femtosecond-pulsed excitation beam. Similar photon densities can be obtained in a planar near-interfacial layer by total internal reflection of a femtosecond-pulsed excitation beam (Fig. 2). From comparison with the Gaussian–Lorentzian excitation volume in 2PEF scanning microscopy, we anticipate:

$$V_{2\omega} \approx \frac{2\pi}{\cos\vartheta} w_r^2 w_z(\vartheta) \quad (2)$$

where $w_z(\vartheta) << w_r$ is the penetration depth and w_r is the beam's half width in the specimen plane at $\vartheta = 0$ (see Appendix). Evanescent wave two-photon fluorescence excitation (EW 2PEF) has the advantage over a focused-spot geometry of reducing the axial extent of the excitation volume to $w_z(\vartheta) \approx \lambda/5$, which permits non-linear fluorescence excitation over a lateral dimension much larger than the waist of a focused beam. Figure 2A shows the measured fluorescence as a function of ϑ for one- (1PEF, top panel) and two-photon excitation (2PEF, bottom). Solid lines indicate, for $\vartheta < \vartheta_c$, the transmitted intensity, calculated from the Fresnel coefficient (squared for 2PEF), and, for $\vartheta \geq \vartheta_c$, the calculated EW field intensity

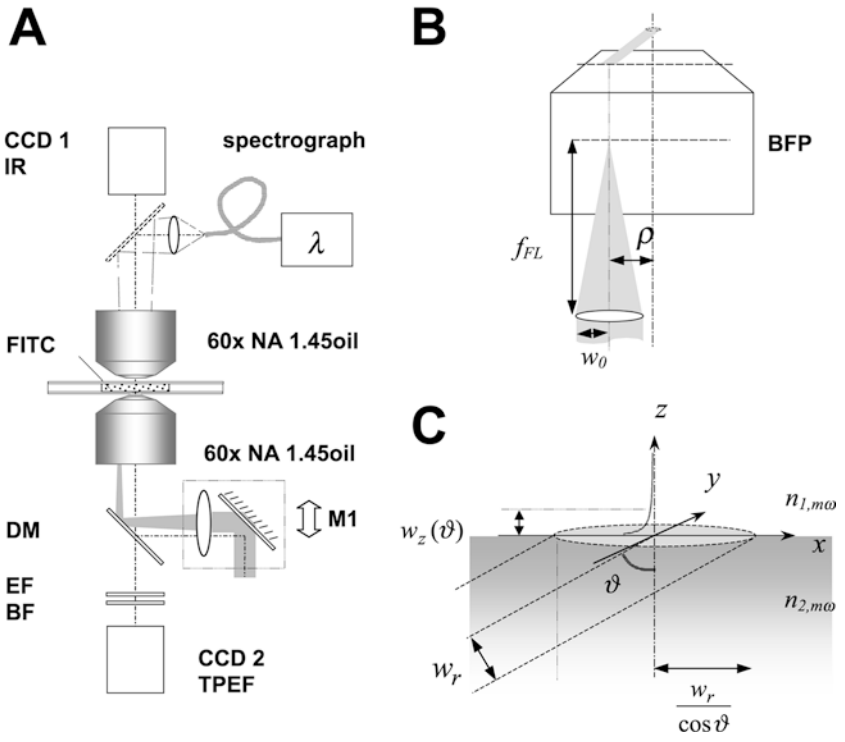

Fig. 1A–C Experimental layout. **A** A beam is focused with lens *L1* in the back focal plane of a high-NA objective. The emerging parallel beam excites fluorescence in a fluorescein solution in a sealed chamber. Lateral displacement of mirror *M1* by a distance allows control of the beam angle ϑ. The resultant fluorescence and transmitted light are detected on a back-illuminated CCD camera and spectrograph, respectively. An infrared camera (*top*) helped to align the axes of both objectives, one of which was mounted on a micrometer-driven *x*,*y* stage. *DM*: dicroic mirror; *EF*: emission filter; *BF*: IR blocking filter. **B** A collimated Gaussian beam with half-width w_r incident at an angle ϑ at a plane dielectric interface ($n_{2,m\omega} > n_{1,m\omega}$) creates an evanescent field with penetration depth $w_z(\vartheta)$ in the *z*-direction, and half-axes w_r and $w_r/\cos\vartheta$, respectively. **C** Spot size w_r and incidence angle ϑ are determined by the focusing angle $\arctan(w_0/f_{FL})$ and the radial beam displacement ρ, respectively

(Axelrod et al. 1984) (squared for 2PEF), respectively. The quadratic dependence of 2PEF on the incident beam intensity results in a surface enhancement of the generated fluorescence for values of $\vartheta \approx \vartheta_c$. Figure 2B shows 2PEF images of the fluorescein sample at supercritical (top) and subcritical beam incidence (bottom, epifluorescence excitation). Evidence for the two-photon nature of fluorescence excitation came from (1) the square dependence of the measured fluorescence intensity on the incident laser power (inset in Fig. 2B); (2) the absence of a signal when de-modelocking the laser (not shown); (3) a spectroscopic scan from 380 to 900 nm, which excluded surface second-harmonic generation as a source of the signal (data not shown).

Two-photon excitation results in a well-defined excitation volume

A Gaussian beam intercepting the reflecting interface at an angle $\vartheta > \vartheta_c$ results in an elongated Gaussian excitation profile with half-widths $w_r/\cos(\vartheta)$ and w_r and penetration depth $w_z(\vartheta)$ (see Appendix). We sampled the fluorescence generated in a 100-μM fluorescein solution and assessed deviations from the calculated spatial intensity distribution. We obtained the peak fluorescence intensity $I_{max}(x)$, background intensity $I_{min}(x)$ and half-width $w_y(x)$ as parameters of consecutive fits of 1-D Gaussians to the measured fluorescence profile along transverse line profiles (along $\boldsymbol{u}_y$; see inset in Fig. 3A). We used these data to calculate the image contrast $C(x;\vartheta) = (I_{max} - I_{min})/(I_{max} + I_{min})$ and the asymmetry parameter $W_y(x;\vartheta) = w_y(x;\vartheta)/(w_r(0;0))$.

Figure 3A (top) shows the measured, strongly skewed, 1PEF excitation profile at an angle just above the critical angle, $\vartheta_c + 1°$. Both the excited fluorescence, $I_{max}(x;\vartheta)$ (measured within the nominal excitation spot, black), and the background fluorescence, $I_{min}(x;\vartheta)$ (grey), increased in the propagation direction of the EW ($\boldsymbol{u}_x$, bottom panel). The spread of excitation decreased with larger beam angles, but 1PEF failed to produce a well-defined Gaussian excitation profile (panel B). Figure 3C illustrates how the spatial excitation profile changes upon EW 2PEF. For values of $\vartheta > \vartheta_c$ close to the critical angle (left panel), we observed a similar behaviour as with 1PEF, probably reflecting imperfect collimation of the incident beam. At larger beam angles, both the localization of fluorescence excitation and its lateral spread were reduced compared to 1PEF (Fig. 3C, middle panel). Two-photon excitation increased the signal-to-background ratio by a factor of four, compared with 1PEF. Part of this improvement stemmed from more efficient optical filtering resulting from the large spectral separation between infrared excitation light and visible 2PEF emission (data not shown). The

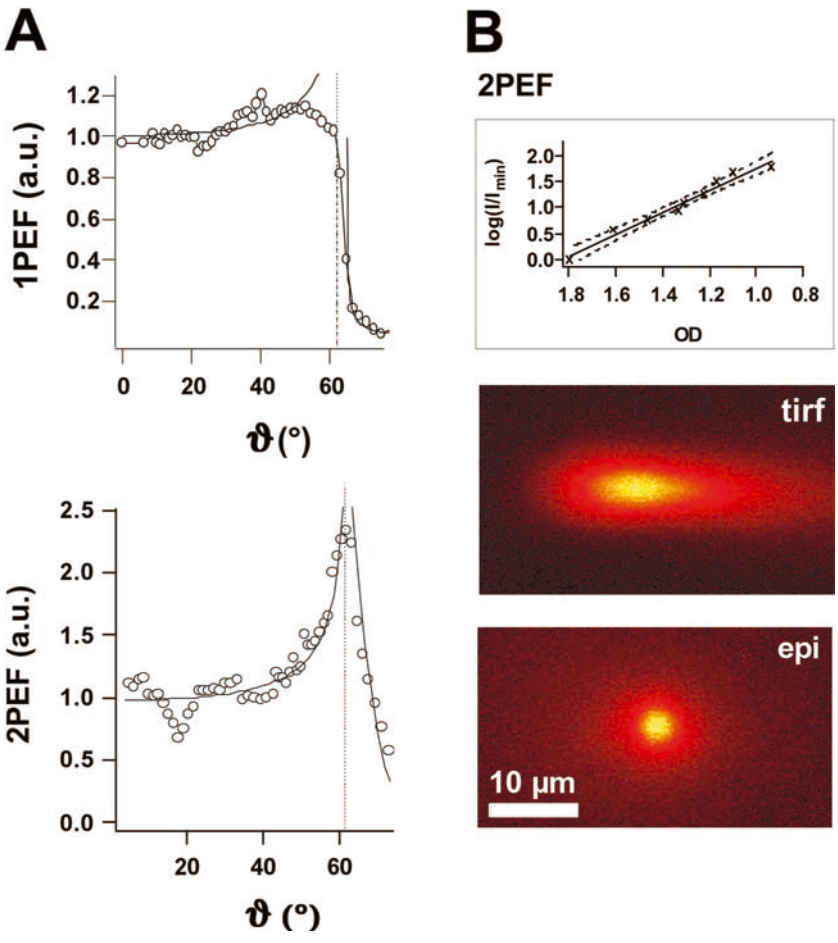

Fig. 2A, B Evanescent wave excitation of two-photon fluorescence (2PEF). **A** Measured 1PEF (*top*) and 2PEF intensities (*bottom*) as a function of ϑ. Intensity normalized to its value at normal beam incidence, $\vartheta = 0°$. 2PEF excitation is near-field enhanced close to $\vartheta_c = 61.9°$ (*dashed line*, calculated critical angle: 62.1°). *Solid lines* show theoretical intensity values (see text). Angle and intensity were measured with $\Delta\vartheta = 1.2°$and $\Delta m\text{PEF} = 0.15$ accuracy, respectively. **B** *Top*: log–log plot of 2PEF intensity vs. fractional incident power (optical density, OD), and best fit (slope of 2.12 ± 0.14) confirming 2PEF. *Below*: 2PEF images at supercritical ($\vartheta_c < \vartheta = 65°$, *upper*) and subcritical beam incidence ($\vartheta = 0°$, *lower*). Gaussian beam widths where 3.68 ± 0.01 µm and 4.29 ± 0.01 µm in *x*- and *y*-directions, for $\vartheta = 0°$ (epifluorescence excitation), and 8.25 ± 0.02 µm, 3.89 ± 0.01 µm for $\vartheta = 65°$, respectively. Images are 10-frame averages; exposure time 100 ms per image

measured two-photon excitation profile approached a Gaussian distribution for penetration depths below $w_{z,2\omega}(\vartheta_c + 5°) = 155$ nm (Fig. 3C, rightmost panel). Some broadening was observed where the incident and reflected beam entered and left the coverslip.

The two-photon EW excitation volume is fairly insensitive to scattering

To understand this degradation of the 1PEF excitation volume, we tested the impact of EW scattering by imaging non-labelled CHO cells embedded in a 100-µM fluorescein-containing extracellular solution (Fig. 4A, top). We chose the size of the elliptical excitation spot to be smaller than the cellular "footprint" so that no extracellular fluorescence should be observed in the absence of scattering. Figure 4 shows the measured fluorescence distribution upon 1PEF (panel A, middle). A comet tail of extracellular fluorescence appears in the propagation direction of the evanescent field, as if forward scattering caused excitation photons to leak into the far field. Our observations corroborate earlier experiments (Rohrbach 2000) and indicate a loss of localized excitation when imaging biological specimens.

If scattered excitation light causes this extracellular fluorescence, non-linear excitation should abolish this signal. Figure 4A (bottom) confirms the restriction of 2PEF to the thin interfacial layer of dye beneath the cell. Furthermore, the amount of extracellular fluorescence should depend on the flow of energy from the higher-index medium (2) to the aqueous medium (1). We tested this prediction by taking advantage of the proportionality of the Goos–Hänchen shift (Artmann 1948; Goos and Hänchen 1947) to the flow of energy (Synder and Love 1976) to the optically rarer medium. Varying ϑ, we systematically varied the displacement resulting from the Goos–Hänchen effect:

$$d_x^{\perp}(\vartheta)/\lambda = \frac{1}{\pi}\frac{\mu \sin\vartheta \cos^2\vartheta}{\mu^2\cos^2\vartheta + \sin^2\vartheta - n^2}\frac{1}{\left(\sin^2\vartheta - n^2\right)^{\frac{1}{2}}} \qquad (3)$$

Equation (3) holds true for the polarization direction of the electric field vector perpendicular to the incidence plane, $\mu = \mu_1/\mu_2 = \mathbf{1}$, $n = n_1/n_2$, and we have neglected the slight dependence of n on λ. Figure 4B (top) quantifies the amount of extracellular 1PEF as a function of ϑ. On the plot of the amount of fluorescence generated in the extracellular space versus $d_x^{\perp}$ (bottom), we recognize a linear relationship for small displacements (large beam angles) and a plateau for values of ϑ approaching ϑ_c.

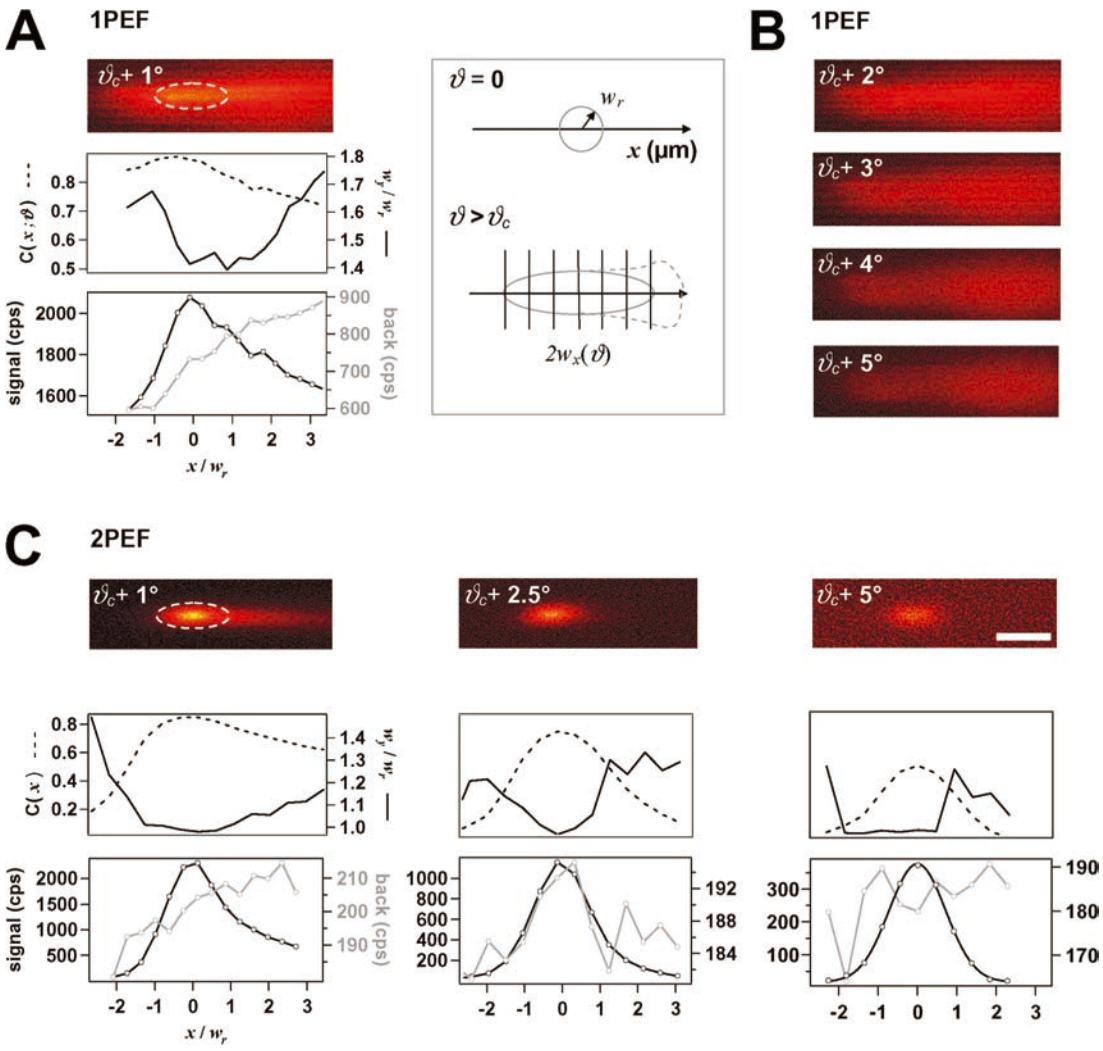

Fig. 3A–C Localization of 2PEF excitation. **A** *Top*: EW 1PEF of a homogenous 100-μM fluorescein sample at $\vartheta_c + 1°$. The excitation volume is much larger than the expected elliptic profile (*white*). *Middle*: image contrast $C(x)$ (*dashed line*) and lateral beam broadening (*solid line*) as a function of normalized distance x/w_r. *Bottom*: signal (*black*) and background (*grey*) as a function of x/w_r. *Right*: quantifying the excitation profile. *Top*: w_r was obtained from a radial sweep of the fluorescence distribution at normal beam incidence, $\vartheta = 0$. *Bottom*: sampling the spatial distribution of fluorescence excitation by successive line profiles in the y-direction. **B** Increasing ϑ does not significantly affect 1PEF flare. ϑ expressed relative to the measured critical angle $\vartheta_{c,mw}$. **C** *Top*: 2PEF images of the same sample. Image contrast and beam broadening (*middle panel*) as well as signal and background (*bottom*), respectively, for 2PEF at different values of ϑ. A perfect Gaussian is observed for large ϑ (small penetration depths). *Scale bar* 5 μm, for all images

The inflection point corresponds to a penetration depth $w_z \approx 150$ nm, corroborating previous observations (Rohrbach 2000). Figure 4D illustrates the dependence of $d_x^{\perp}$ and w_z on ϑ. The Goos–Hänchen shift is of the order of the excitation wavelength, and, like the penetration depth w_z, is maximal for values of ϑ close to ϑ_c (Fig. 4D).

In summary, Fig. 4 demonstrates the dependence of the light confinement of the EW on the amount of scattered excitation light. With 1PEF, shallow penetration can offer a way to localize EW excitation. For deeper penetration, scattering compromises the light confinement. As expected from the threshold behaviour of two-photon absorption, extracellular fluorescence is almost completely absent with non-linear excitation.

We illustrate the localized excitation of EW 2PEF by imaging secretory vesicles, fluorescently labelled with the acidic compartment marker acridine orange (AO). Owing to the high density of secretory vesicles and their refractive-index difference compared to the cytoplasm (Oheim et al. 1998; Steyer et al. 1997), chromaffin cells provide a highly scattering and non-uniform fluorescent sample (Fig. 5A). The 2PEF image (top panel, $\lambda_{ex} = 860$ nm) is crisper and more contrasted than the corresponding 1PEF image, taken a few milliseconds later with equal probe depth $w_{z,\omega} = \frac{1}{2} w_{z,2\omega} \approx 110$ nm (bottom, $\lambda_{ex} = 488$ nm). As expected from the square dependence of 2PEF on the incident EW intensity, the depth penetration of both excitation modes appears comparable; no additional features located at deeper cellular regions are seen on the EW 2PEF image.

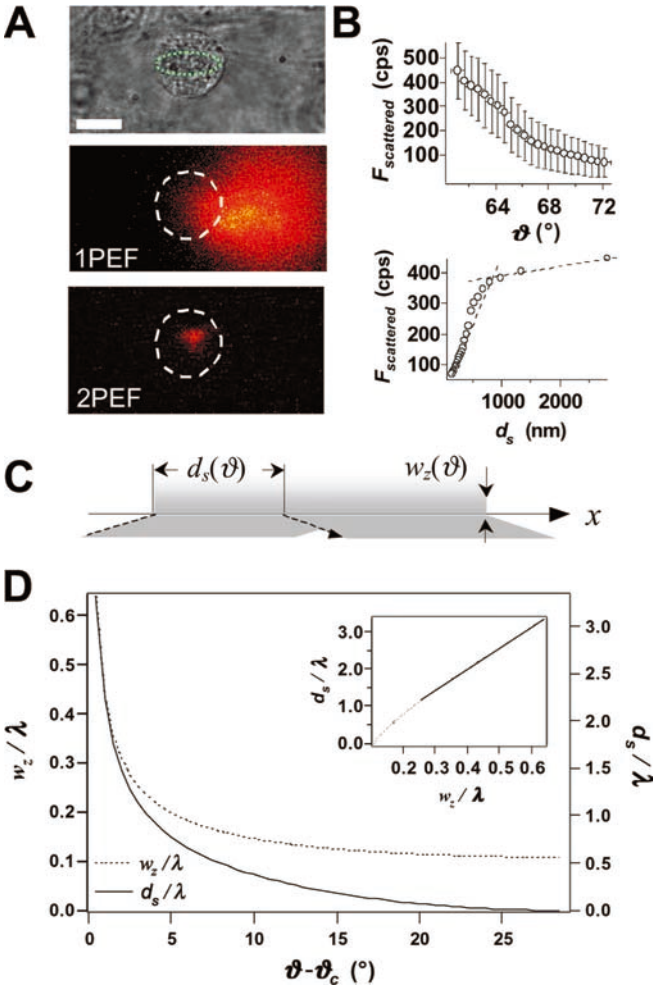

Fig. 4A–D EW scattering at the bottom of a cell. **A** *Top*: bright-field transmission image of a CHO cell. Scale bar 15 μm; exposure time 5 ms. *Middle and bottom*: ''negative staining'' of the extracellular space with 100- μM FITC dextran reveals a significant flare of scattered one-photon excitation in the propagation direction of the EW (*middle*). The requirement for simultaneous two-photon absorption results in an almost complete suppression of fluorescence excitation by scattered photons (*bottom*); 100-ms exposure. Images scaled to equal brightness at 590 and 280 cps fluorescence intensity. **B** Plot of the extracellular 1PEF (mean ± standard deviation) vs. ϑ (*top*), and vs. the Goos–Hänchen displacement. **C** The reflected beam (*dashed arrow*) is laterally displaced with respect to the incoming beam as a consequence of the Goos–Hänchen effect. **D** Normalized calculated penetration depth w_z and lateral beam displacement d_s as a function of ϑ. Inset: $d_s \approx 6.75 w_z$, for $\vartheta >> \vartheta_c$, independent of λ

In addition to providing high-resolution images of a thin sub-membrane section, EW 2PEF offers the advantage of simultaneous excitation of several fluorophores. We illustrate this by imaging GFP-GPI/actin-phalloidin double-labelled fibroblasts. Dual-colour epifluorescence recordings confirmed GFP expression and actin labelling (Fig. 5C). We verified cellular adhesion to the coverglass with 488/568-nm EW imaging (panel D). Cells were fixed and transferred to the EW 2PEF microscope. Figure 5E and Fig. 5F show 488-nm EW 1PEF and 2PEF evanescent wave excitation. We recognize two growth cones facing each other.

Discussion

The limited depth penetration of the evanescent field into the lower-index medium creates the conditions for fluorescence excitation in the immediate proximity of a dielectric interface (Axelrod et al. 1984). Scattering compromises this localized excitation, e.g. when imaging cells grown on a coverslip (Fig. 3). Scattering spatially redistributes excitation photons and adds a far-field component to the excited fluorescence. The sensitivity of EW excitation to scattering can be explained by taking into account the distance $d_x^{\perp}$ of EW propagation parallel to the reflecting interface. Although $d_x^{\perp}$ is of the order of λ (Artmann 1948; Goos and Hänchen 1947) and is much smaller than the scattering mean free path $l_s^{(\lambda)}$, which is of the order of 10–100 μm (Tuchin 2000), Monte-Carlo simulations indicate that scattering of a few photons suffices to produce the observed far-field excitation of fluorescence (unpublished data).

Multiphoton laser-scanning microscopy (Denk et al. 1990) is known to offer a distinct advantage when the major limitation on image contrast is background noise (Denk and Svoboda 1997). Restriction of the two-photon excitation volume to the near-interfacial region defined by the EW permits planar 2PEF over a micrometer-sized surface area without the necessity for beam scanning. Part of this advantage derives from the local-field enhancement of the EW. The effective probe distances are roughly equal with EW 1PEF and 2PEF, as the larger penetration depth of the infrared excitation light is compensated for by the square dependence of the amount of generated fluorescence on the incident intensity. Previous work has exploited non-linear EW excitation for non-linear spectroscopy of sodium atoms at a gas/solid boundary (Bordo et al. 2001), for analytical chemistry (Gryczynski et al. 1997), two-photon pattern photobleaching (Huang and Thompson 1993) and EW-excited second-harmonic generation (SHEW) at the interface of linear and non-linear media (Bloembergen and Lee 1968; see Kiguchi et al. 1992, and references therein). The present experiments were designed to illustrate the benefits of EW 2PEF for biological imaging. Our experiments demonstrate non-scanning (planar) two-photon fluorescence excitation in a total internal reflection geometry. We demonstrate EW 2PEF through the margins of a high-NA objective lens (Caldwell 1997; Kawano et al. 2001; Stout and Axelrod 1989), a geometry that is preferred since it permits experimental access to the cells. The micrometer-sized 2PEF excitation spot allows imaging small cells or sub-regions of larger branched cells without beam scanning.

A major advantage that derives from non-linear EW excitation is reduced flare due to the inefficiency of scattered excitation light exciting 2PEF. While this

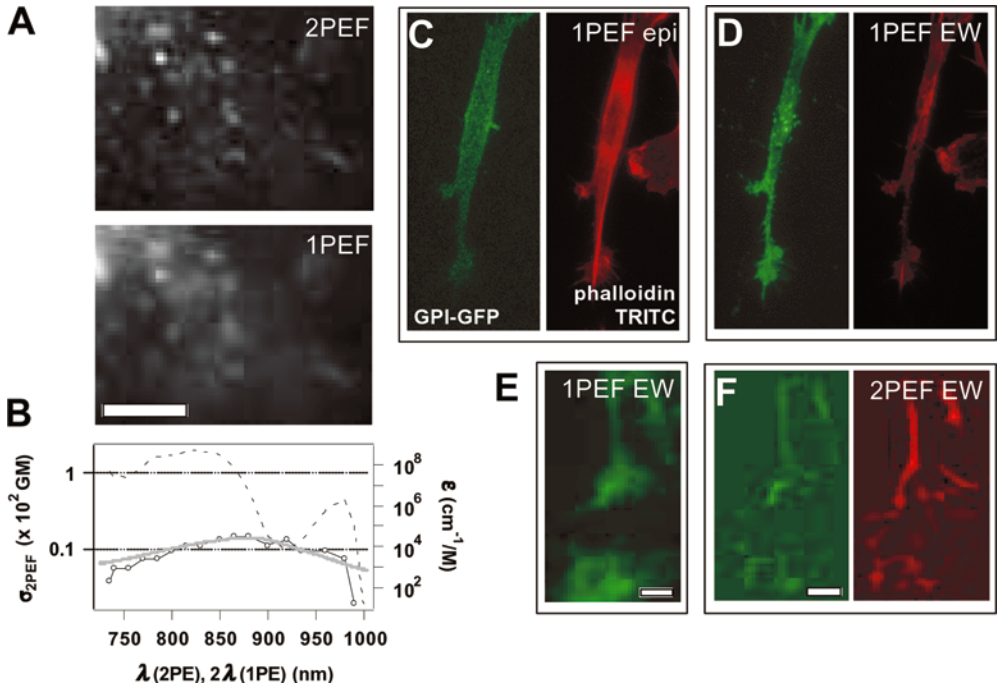

Fig. 5A–F Two-photon evanescent wave excitation of cellular fluorescence. 860-nm 2PEF (*top*) and 488-nm 1PEF (*bottom*) images of an acridine orange (AO) labelled chromaffin granules at equal probe depth ~110 nm. Scale bar 5 μm; integration times were 100 ms each; images represent subsequent frames, with <3 ms inter-frame interval. **B** AO 2PEF spectrum (*solid line*), together with that of rhodamine B (*dashed line*) and the AO molar extinction (*grey*), the latter plotted against 2λ for direct comparison. 2PEF curves were normalized to the two-photon absorption cross-section $\sigma_{2PEF} = 200$ GM (10^{-50} cm^4 s/photons) of rhodamine B at 840 nm; $\epsilon(2\lambda)$ was normalized to have an extinction coefficient of 27,000 cm^{-1} M^{-1} at 431 nm (Ferguson and Mau 1972). For AO, we find $\sigma_{2PEF} \approx 15$ GM at 860 nm. One-photon 480/560-nm epifluorescence (**C**) and 488/568-nm evanescent wave excited (**D**) fluorescence images of GPI-GFP/actin-phalloidin TRITC double-labelled 3T3 fibroblasts. GPI is a lipid-raft marker and located at the plasma membrane, whereas phalloidin labels cytoskeletal F-actin. Images were taken with an intensified PentaMax camera (Princeton Instruments; pixel size in the specimen plane = 188 nm; NA 0.9). Note the increase in contrast and near-membrane detail upon EW excitation. **E** GPI-GFP EW 1PEF image of a fixed fibroblast from the same preparation as above, showing two growth cones face-to-face; scale bar 1 μm. **F** EW 2PEF image at 900-nm excitation of the same cell as shown in **E**, with fluorescence detected at 505–530 nm (*left*) and 610–680 nm, respectively; pixel size 108 nm; NA 1.45

advantage over 1PEF EW microscopy is already observed for cuvette measurements (Fig. 3), we demonstrate that EW scattering is the dominant factor in shaping the excitation volume when imaging a scattering sample (Fig. 4). A second advantage that derives from EW 2PEF is the simultaneous excitation of multiple fluorophores (see Fig. 5), which is required when studying heterogeneous systems, the interaction of reaction partners or the co-localization of fluorophores, one of the most promising of the recent developments in EW imaging (Keller et al. 2001; Tsuboi et al. 2000). Although conventional techniques for multiparameter imaging such as fluorescence-lifetime EW measurements (Bicknese et al. 1993; Toriumi and Masuhara 1991) are reliable, they typically have a lower signal-to-noise ratio at the (video) frame rates often required for studying subcellular dynamics. As with multifocal 2PEF imaging (Bewersdorf et al. 1998), an imaging detector has to be used for 2PEF EW microscopy, resulting in some resolution loss due to the scattering of the generated fluorescence, a problem that is absent from whole-field detection schemes using single-spot scanning. We finally note that through-the-objective EW excitation of 2PEF requires focusing a pulsed laser beam in the objective's back focal plane. The objective's destruction threshold therefore prescribes a limit to the maximum power. We observed no damage up to average laser powers of 8 mW, corresponding to ~0.1 nJ per pulse. EW 2PEF provides a powerful set-up for background-free, quantitative, high-resolution imaging of subcellular detail in scattering samples.

Acknowledgements We thank T. Pons and G. Bunt for help with some experiments, J.-S. Schonn and C. Chapuis for chromaffin cell preparation and B. Babour for comments on the manuscript. Supported by the French Ministry of Research and Technology (M.N.R.E.T.) (ACI "jeunes chercheurs" no. 5242, to M.O.) and a Studienstiftung fellowship to F.S.

Appendix

Two-photon evanescent wave excitation volume

Assuming no stimulated emission or self-quenching, the number of fluorescence photons collected per unit time following a m^{th}-order excitation process is given by:

$$F(t) = \frac{1}{2}\phi\eta_{m\omega}\left(\sigma_{m\omega}\int_V I^m(\mathbf{x},t)C(\mathbf{x},t)\,\mathrm{d}\mathbf{x}\right) \tag{A1}$$

where ϕ, $\eta_{m\omega}$, σ_m and C are the collection efficiency, the quantum efficiency, m-photon excitation cross-section and the fluorophore concentration, respectively. The term in brackets is the number of absorbed photons. In the absence of saturation and photobleaching, $F(t) \propto I^m(t)$ and $C(\boldsymbol{x},t) = C = \text{const}$. Let $W(\boldsymbol{x})$ and $I(t)$ denote the spatial and temporal excitation profile. We further introduce a volume contrast:

$$\gamma_{m\omega} = \int_V W_{m\omega}^2(x)\,\mathrm{d}x \Big/ \int_V W_{m\omega}(x)\,\mathrm{d}x \tag{A2}$$

Then:

$$F(t) = \frac{1}{2}\phi\eta_{m\omega}\sigma_{m\omega}CI^m(t)\left(\gamma_{m\omega}^{-1}\int_V W_{m\omega}(\mathbf{x})\,\mathrm{d}\mathbf{x}\right) \tag{A3}$$

where the term in brackets denotes the excitation volume, $V_{m\omega}$. In practice, we only measure the time-averaged photon flux $\langle F(t)\rangle$:

$$\langle F(t)\rangle = \frac{1}{2}c_{m\omega}\langle I(t)\rangle^m V_{m\omega} \tag{A4}$$

where $\phi\eta_{\mathrm{m}\omega}\sigma_{\mathrm{m}\omega}\mathrm{C}$ and the m^{th}-order temporal coherence $g = \langle I^m(t)\rangle/\langle I(t)\rangle^m$ are combined to a fluorophore and instrument parameter $c_{m\omega}$. The average fluorescence is proportional to the average intensity raised to the m^{th} power and the m-photon excitation volume.

In the case of m-photon evanescent-field excitation, the beam's half width w_r and the angle of incidence ϑ at the reflecting interface ($n_{2,m\omega} > n_{1,m\omega}$) determine the spatial excitation profile, $W_{m\omega}(r) \propto \exp\left(-mr^2\cos\vartheta/2w_r^2\right)$ and $W_{m\omega}(z) \propto \exp(-mz/w_z(\vartheta))$. Here r and z denote distances within and perpendicular to the interface plane, respectively, w_r is the half-width of the illumination beam in the specimen plane at normal incidence ($\vartheta = 0$), and $w_z(\vartheta) = \lambda\Big/\left(4\pi(n_2^2\sin^2(\vartheta) - n_1^2)^{1/2}\right)$ is the distance over which the evanescent-field intensity decays to $1/e$ of its value at the reflecting interface at $z = 0$ (typically called "penetration depth"). For through-the-objective EW excitation, w_r and ϑ can be approximated as: $\emptyset_{\mathrm{pupil}}w_0/(2f_{\mathrm{FL}})$ and $\arcsin\left(M\rho/(n_{2,m\omega}f_{\mathrm{TL}}\right)$, respectively. $\emptyset_{\mathrm{pupil}}$, M and $n_{2,m\omega}$ denote the diameter of the objective's back pupil, magnification and refractive index of the immersion medium, respectively, w_0 is the beam's half-width at the focusing lens, and f_{FL} and f_{TL} are the focal lengths of the focusing lens and tube lens, respectively (see Fig. 1); ρ denotes a radial displacement of the focused beam relative to the optical axis.

Substituting the expressions for $W(r)$ and $W(z)$ into Eqs. (A2) and (A3) and integrating over a volume element $r\mathrm{d}r\mathrm{d}\varphi\mathrm{d}z$ we obtain $\int W_{m\omega}(x)\,\mathrm{d}x \propto 2\pi w_r^2 w_z(\vartheta)\big/\left(m^2\cos(\vartheta)\right)$ and $\gamma = \frac{1}{4}$, independent of m. Thus for non-linear evanescent-field fluorescence excitation, the excitation volume is given by:

$$V_{m\omega} \approx \frac{8\pi}{m^2\cos(\vartheta)}w_r^2 w_z(\vartheta) \tag{A5}$$

Substituting in Eq. (A4):

$$\langle F(t)\rangle = \frac{4\pi c_{m\omega}w_r^2}{m^2\cos(\vartheta)}\langle I(t)\rangle^m w_z(\vartheta) \tag{A6}$$

from which we note that the total generated fluorescence is proportional to $w_z(\vartheta)$. We can thus determine, at a beam angle ϑ, $w_z(\vartheta)$ from a linear fit to a plot of $\langle F(t)\rangle$, normalized by instrument and fluorophore parameters, versus the average EW intensity raised to the m^{th} power.

How does Eq. (A5) compare with the excitation volume in two-photon scanning microscopy? For the Gaussian–Lorentzian intensity profile of a tightly fo cused excitation beam: $V_{2\omega}^{(\mathrm{GL})} = \frac{16}{3}\pi^2 w_r^2 z_0$ and $\gamma = \frac{3}{16}$ (Mertz 1998). We approximate $w_r \approx 0.26\lambda/\sin\vartheta_{\mathrm{NA}}$ and $z_0 = 4\pi w_r^2/\lambda$ is the Rayleigh length, where $\mathrm{NA} > 0.8$ has been assumed. ϑ_{NA} is the half-angle spanned by the NA. Thus, for a 0.9-NA water immersion objective, $V_{2\omega}^{(\mathrm{GL})} \approx 7$ fl. To observe 2PEF upon EW excitation with $w_z \approx 0.2$ μm at comparable levels of incident power, we hence need to restrict the lateral spot size to $w_r \approx 3$ μm, close to what was observed experimentally (Fig. 2B). As fluorescence is excited within a volume section of $w_z(\vartheta)/m$ thickness, the *effective* excitation depth in one and multiphoton EW microscopy are equal, for excitation of the same fluorophore.

References

Artmann K (1948) Berechnung der Seitenversetzung des Totalreflektierten Strahles. Ann Phys 6:87–102

Axelrod D (1989) Total internal reflection fluorescence microscopy. Methods Cell Biol 30:245–270

Axelrod D (2001a) Selective imaging of surface fluorescence with very high aperture microscopy objectives. J Biomed Opt 6:6–13

Axelrod D (2001b) Total internal reflection fluorescence microscopy in cell biology. Traffic 2:764–774

Axelrod D, Burghardt TP, Thompson NL (1984) Total internal reflection fluorescence. Annu Rev Biophys Bioeng 13:247–268

Bewersdorf J, Pick R, Hell SW (1998) Multifocal multiphoton microscopy. Opt Lett 23:1–3

Bicknese S, Perasamy N, Shohet SB, Verkman AS (1993) Cytoplasmic vicosity near the cell plasma membrane: measurement by evanescent field frequency domain microfluorimetry. Biophys J 65:1272–1282

Bloembergen N, Lee CH (1968) Total reflection in second-harmonic generation. Phys Lett 19:835–837

Bordo VG, Loerke J, Rubahn H-G (2001) Two-photon evanescent-volume wave spectroscopy: a new account of gas-solid dynamics in the boundary layer. Phys Rev Lett 86:1490–1493

Caldwell JB (1997) Ultra high NA microscope objective. Opt Photonics News 11:44–46

Chew H, Wang D-S, Kerker M (1979) Elastic scattering of evanescent electromagnetic waves. Appl Opt 18:2679–2687

Darchen F, Zahraoui A, Hammel F, Monteils MP, Tavitian A, Scherman D (1990) Association of the GTP-binding protein

Rab3A with bovine adrenal chromaffin granules. Proc Natl Acad Sci USA 87:5692–5696
Denk W, Svoboda K (1997) Photon upmanship: why multiphoton imaging is more than a gimmick. Neuron 18:351–357
Denk W, Strickler JH, Webb WW (1990) Two-photon laser scanning fluorescence microscopy. Science 248:73–76
Epstein JR, Brian I, Walt DR (2002) Fluorescence-based nucleic acid detection and microarrays. Anal Chim Acta 469:3–36
Ferguson J, Mau AWH (1972) Absorption studies of acid-base equilibria of dye solutions. Chem Phys Lett 17:543–546
Funatsu T, Harada Y, Higuchi H, Tokunagag M, Saito K, Ishii Y, Vale RD, Yanagida T (1997) Imaging and nano-manipulation of single biomolecules. Biophys Chem 68:63–72
Goos F, Hänchen H (1947) Ein neuer und fundamentaler Versuch zur Totalreflexion. Ann Phys 6:333–346
Gryczynski I, Gryczynski Z, Lakowicz JR (1997) Two-photon excitation by the evanescent wave from total internal-reflection. Anal Biochem 247:69–76
Harrick NJ (1967) Internal reflection spectroscopy. Wiley, New York
Huang Z, Thompson NL (1993) Theory for two-photon excitation in pattern photobleaching with evanescent illumination. Biophys Chem 47:241–249
Kawano Y, Abe C, Kaneda T, Aono Y, Abe K, Tamura K, Terakawa S (2001) High-numerical aperture objective lenses and optical system improved objective-type total internal reflection fluorescence microscopy. Proc SPIE XX:142–153
Keller P, Toomre D, Diaz E, White J, Simons K (2001) Multicolor imaging of post-Golgi sorting and trafficking in live cells. Nat Cell Biol 3:140–149
Kiguchi M, Kato M, Okunaka M, Tnaiguchi Y (1992) New method of measuring second harmonic generation efficiency using powder crystals. Appl Phys Lett 60:1933–1935
Loerke D, Stühmer W, Oheim M (2002) Quantifying axial secretory-granule motion with variable-angle evanescent-field excitation. J Neurosci Methods 119:65–73
Mertz J (1998) Molecular photodynamics involved in multi-photon excitation fluorescence microscopy. Eur Phys J D 3:53–66
Mertz J (2000) Radiative absorption, fluorescence and scattering of a classical dipole near a lossless interface: a unified description. J Soc Opt Am B 17:1906–1913
Oheim M, Stühmer W (2000) Tracking individual granules through the actin cortex. Eur Biophys J 29:67–89
Oheim M, Loerke D, Stühmer W, Chow RH (1998) The last few milliseconds in the life of a secretory granule. Docking, dynamics and fusion visualized by total internal reflection fluorescence microscopy (TIRFM). Eur Biophys J 27:83–98
Rohrbach A (2000) Observing secretory granules with a multiangle evanescent wave microscope. Biophys J 78:2641–2654
Seitz A, Kojima H, Oiwa K, Mandelkow EM, Song YH, Mandelkow E (2002) Single-molecule investigation of the interference between kinesin, tau and MAP2c. EMBO J 21:4896–4905
Snyder AW, Love JD (1976) Goos-Hänchen shift. Appl Opt 15:236–238
Sonnleitner A, Mannuzzu LM, Terakawa S, Isacoff EY (2002) Structural rearrangements in single ion channels detected optically in living cells. Proc Natl Acad Sci USA 99:12759–12764
Steyer JA, Almers W (2001) A real-time view of life within 100 nm of the plasma membrane. Nat Rev Cell Biol 2:268–275
Steyer JA, Horstmann H, Almers W (1997) Transport, docking and exocytosis of single secretory granules in live chromaffin cells. Nature 388:474–478
Stout AL, Axelrod D (1989) Evanescent field excitation of fluorescence by epi-illumination microscopy. Appl Opt 28:5237–5242
Thompson NL, Lagerholm BC (1997) Total internal reflection fluorescence: applications in cellular biophysics. Curr Opin Biotechnol 8:58–64
Thompson NL, Pearce KH, Hsieh HV (1993) Total internal reflection fluorescence microscopy: application to substrate-supported planar membranes. Eur Biopyhs J 22:367–378
Toomre D, Manstein DJ (2001) Lightning up the cell surface with evanescent wave microscopy. Trends Cell Biol 11:296–303
Toriumi M, Masuhara H (1991) Time-resolved total internal reflection fluorescence spectroscopy: principles, instruments and applications. Spectrochim Acta Rev 14:353–377
Tsuboi T, Zhao C, Terakawa S, Rutter GA (2000) Simultaneous evanescent wave imaging of insulin vesicle membrane and cargo during a single exocytic event. Curr Biol 10:1307–1310
Tuchin V (2000) Tissue optics. Light scattering methods and instruments for medical diagnosis, vol TT38. SPIE Press, Bellingham